

## **Radiation Damage in the Ultra-Wide Bandgap Semiconductor Ga<sub>2</sub>O<sub>3</sub>**

Xinyi Xia<sup>1</sup>, Jian-Sian Li<sup>2</sup>, Ribhu Sharma<sup>2</sup>, Fan Ren<sup>1</sup>, Md Abu Jafar Rasel<sup>3</sup>, Sergei Stepanoff<sup>4</sup>, Nahid Al-Mamun<sup>3</sup>, Aman Haque<sup>3</sup>, Douglas E. Wolfe<sup>4</sup>, Sushrut Modak<sup>5</sup>, Leonid Chernyak<sup>5</sup>, Mark E. Law<sup>6</sup>, Ani Khachatrian<sup>7</sup> and S. J. Pearton<sup>2</sup>

<sup>1</sup> Department of Chemical Engineering, University of Florida, Gainesville, FL 32606 USA

<sup>2</sup> Department of Materials Science and Engineering, University of Florida, Gainesville, FL 32606 USA

<sup>3</sup> Department of Mechanical Engineering, Penn State University, University Park, PA 16802, USA

<sup>4</sup> Department of Materials Science and Engineering, Penn State University, University Park, PA 16802, USA

<sup>5</sup> Department of Physics, University of Central Florida, Orlando, FL 32816, USA

<sup>6</sup> Department of Electrical and Computer Engineering, University of Florida, Gainesville, Florida 32611

<sup>7</sup> US Naval Research Laboratory, 4555 Overlook Ave., S.W. Washington, DC 20375, USA

### **Abstract**

Ga<sub>2</sub>O<sub>3</sub> is expected to show similar radiation resistance as GaN and SiC, considering their average bond strengths. However, this is not enough to explain the orders of magnitude difference of the relative resistance to radiation damage of these materials compared to GaAs and dynamic annealing of defects is much more effective in Ga<sub>2</sub>O<sub>3</sub>. Octahedral gallium monovacancies are the main defects produced under most radiation conditions because of the larger cross-section for interaction compared to oxygen vacancies. Proton irradiation introduces two main paramagnetic defects in Ga<sub>2</sub>O<sub>3</sub>, which are stable at room temperature. Charge carrier

removal can be explained by Fermi-level pinning far from the conduction band minimum due to gallium interstitials ( $Ga_i$ ), vacancies ( $V_{Ga}$ ), and antisites ( $Ga_O$ ). With few experimental or simulation studies on single event effects (SEE) in  $Ga_2O_3$ , it is apparent that while other wide bandgap semiconductors like SiC and GaN are robust against displacement damage and total ionizing dose, they display significant vulnerability to single event effects at high Linear Energy Transfer (LET) and at much lower biases than expected. We have analyzed the transient response of  $\beta$ - $Ga_2O_3$  rectifiers to heavy-ion strikes via TCAD simulations. Using field metal rings improves the breakdown voltage and biasing those rings can help control the breakdown voltage. Such biased rings help in the removal of the charge deposited by the ion strike.

## Introduction

Radiation damage in wide bandgap semiconductors is attracting increasing interest, especially in GaN<sup>(1-16)</sup>. Recently, it has become clear that  $\beta$ -Ga<sub>2</sub>O<sub>3</sub> is attractive for high temperature applications in harsh environments that cannot be tolerated by conventional electronics<sup>(17-29)</sup>. Its wide bandgap allows operation at elevated temperatures, while it is also radiation hard and may provide improved performance over GaN<sup>(30-44)</sup>. Radiation tolerance is an important factor while fabricating microelectronics and typical radiation damage suffered includes total dose effects, displacement damage, and single event effects<sup>(45-67)</sup>. While significant work has been done for radiation effects in GaN<sup>(1-16, 61)</sup> and SiC<sup>(45-60, 62-67)</sup>, the understanding of carrier removal rates, defect levels and annealing regimes for Ga<sub>2</sub>O<sub>3</sub> is ongoing<sup>(68-74)</sup>.

Spacecraft operating beyond Earth's magnetosphere are subject to space weather including the solar wind, a flux of radiation and charged particles that can degrade electronics<sup>(75)</sup>. These charged particles from the solar wind are also trapped inside the Earth's magnetosphere, forming the Van Allen radiation belts, which further expose transiting spacecraft to concentrated levels of charged particles and high-energy radiation<sup>(75)</sup>. An understanding of the radiation damage introduction mechanisms and the damage thresholds in terms of flux, radiation type and energy is needed for next generation semiconductors that will comprise the electronics and sensors capable of operation in harsh environments<sup>(75)</sup>.

Wide-bandgap semiconductor (e.g. GaN and SiC currently and potentially Ga<sub>2</sub>O<sub>3</sub> in future) devices are increasingly used in space and defense systems for embedded high-performance computing and high-throughput I/O processing<sup>(17-19, 76-86)</sup>. A critical issue for many devices is the transient ionization-induced processes associated with high linear energy transfer (LET) particles

and intense pulses of photons. The confined dimensions ( $< 10$  nm radius in the case of charged particles), short time frame (0.1 to 100 ps) and extreme temperatures (1000 to 10,000 degrees) of the ionization-induced thermal spike defy simple dynamics or thermally activated descriptions yet can impact defect production and device degradation. Even the strike of a single ion can produce free charges and defects through ionization in the electrical devices, which can permanently (or temporarily) disrupt device functionality. The effects of ionizing radiation on electronics result from phenomena that occur across time and length-scales. Modeling and simulation approaches provide a range of tools across the scales that can be used to understand the impact of radiation. Defect generation and charge transition are the fundamental mechanisms that govern radiation effects and mitigation in electronic materials <sup>(87-96)</sup>.

Defect production may vary depending on the type of radiation, from high energy ion irradiation and intense pulsed laser irradiation to simulate SEEs from cosmic/solar radiation or intense x-ray bursts. Measuring the response of wide bandgap materials to single-ion events is extremely challenging and two experimental approaches are generally employed (i) measurement of the material response to a large number of non-overlapping ion events of identical energy to obtain an average response or damage state for ions of specific energy; and (ii) direct measurement of material response to single-ion events, one ion at a time. At low ion fluences (between  $10^{10}$  and  $10^{12}$  ions/cm<sup>2</sup>, depending on ion energy and mass), damage regions from individual ions do not overlap and the response to ions of specific mass and energy can be characterized using the known density of ion events and a variety of techniques to determine the nature and concentration of damage/defects.

### **Polytypes of Ga<sub>2</sub>O<sub>3</sub>**

While most attention has concentrated on the thermodynamically stable  $\beta$ -Ga<sub>2</sub>O<sub>3</sub> phase since it can be grown both as single crystals and in epitaxial form and can be alloyed with Al or In to modulate bandgap, there are two other polytypes of interest <sup>(17-20)</sup>. The lattice structures of the three most useful polytypes are shown schematically in Figure 1. The bandgap of the  $\alpha$ -polytype (5.2eV) is larger than that of the  $\beta$  (4.9 eV) drawbacks and does not have the asymmetric thermal conductivity and electrical and optical properties of the latter. Similarly, the  $\varepsilon$ -polytype is ferroelectric and has a high spontaneous polarization, attractive for achieving high 2-dimensional electron gas density. There is much less known about the response of these other two polytypes to radiation, especially the  $\varepsilon$ -polytype <sup>(20)</sup>.

For studying the effects of radiation, we have generally employed either thin films or vertical rectifier structures as our standard device platform, since these enable measurements of most parameters of interest in quantifying the effects of damage <sup>(97-105)</sup>. A typical rectifier structure is shown in Figure 2. It consists of a thick, lightly doped epitaxial layer grown on a conducting substrate. Edge termination generally consists of a dielectric overlap at the edge of the rectifying contact.

**(i) Total Dose Damage**

Since Ga<sub>2</sub>O<sub>3</sub> devices and more generally all wide bandgap semiconductor devices normally use metal gates, Total Ionizing Dose (TID) effects are not as important as they are in Si technology <sup>(42,68-72)</sup>, which is based on MOS-gate devices. The relations between charge (e) and electric field, E (Poisson's equation) and the transport (drift/diffusion) equations depend on carrier mobility ( $\mu_{e,p}$ ) and density (n,p), i.e.,

$$J_n = e\mu_n nE - ED_n \nabla n$$

$$J_p = e\mu_p pE - ED_p \nabla p$$

The current, I, in a rectifier is given by,

$$I = I_0 \left( e^{\frac{eV}{nkT}} - 1 \right)$$

While the similar expression for a lateral field effect transistor is the current between source and drain is given by,

$$I_{DS} = W e n_s v(x)$$

where W is the channel width,  $n_s$  is sheet carrier density and  $v(x)$  is carrier velocity at position x.

Note that in both the lateral and vertical devices, the current depends on carrier concentration and mobility. Displacement damage from radiation creates traps that remove carriers from the conduction process and degrade mobility, i.e.,  $n$ ,  $\mu$  are reduced. These mechanisms are shown schematically in Figure 3.

### **(ii) Radiation-Induced Defects**

A useful parameter for comparing the relative amount of change in electrical properties in irradiated semiconductors is the carrier removal rate,  $R_C$ , defined by <sup>(42,68-70)</sup>:

$$R_C = (n_{s0} - n_s) / \Phi$$

where  $\Phi$  is the proton fluence,  $n_{s0}$  is initial carrier concentration, and  $n_s$  is the irradiated carrier concentration.

The concentration of created vacancies  $N_V$  given by,

$$N_{VGa} = \sigma_{Ga} N_{Ga} \Phi$$

$$N_{VO} = \sigma_O N_O \Phi$$

where  $\sigma_{Ga/O}$  are the cross sections for ion interaction with the lattice ions,  $N_{Ga/O}$  are the concentrations of the corresponding lattice ions, and  $\Phi$  is the fluence, i.e., the number of ions per unit area of the sample. An example calculation for cross-sections of Ga and O atoms to electron

irradiation of different energy is given in Figure 4. Note that for most energies, there will be mainly Ga atoms displaced, ie creation of Ga vacancies,  $V_{\text{Ga}}$  <sup>(106-108)</sup>.

Oxygen vacancies  $V_{\text{O}}$  in  $\text{Ga}_2\text{O}_3$  predicted to be deep donors, whereas Gallium vacancies  $V_{\text{Ga}}$  are predicted to be deep acceptors <sup>(17-20)</sup>. On the basis of the  $\sigma_{\text{Ga/O-Ee}}$  data in Figure 4, we expect ion irradiation with energy less than 0.5-MeV would exclusively produce donor-type doping by oxygen vacancies. For  $> 2.5$ -MeV beam energy, irradiation simultaneously produces  $V_{\text{Ga}}$  and  $V_{\text{O}}$ . The rate of creation of  $V_{\text{Ga}}$  is about twice that of  $V_{\text{O}}$ . The formation energy of  $V_{\text{Ga}}$  is sufficiently low for it to be incorporated in sizeable concentrations during growth, particularly under O-rich and n-type conditions <sup>(17-20)</sup>. The thermodynamic (2-/3-) transition levels of the five different  $V_{\text{Ga}}$  configurations are predicted between  $E_{\text{C-}}$  (1.7- 2.6) eV.  $V_{\text{Ga}}$  can form stable complexes with shallow donor impurities such as H and  $\text{Si}_{\text{Ga}}$  and the  $V_{\text{Ga}}\text{-2H}$  complex has been assigned to an IR absorption line  $3436 \text{ cm}^{-1}$  <sup>(94)</sup>. Complexing  $V_{\text{Ga}}$  with shallow single donors will successively passivate its acceptor levels, shifting luminescence to higher energies.

### **(iii) Energy Deposition and Range Parameters.**

A sometimes-confusing aspect of radiation damage in semiconductors is that a different terminology is employed for the same quantities. Linear Energy Transfer (LET) is used for total or electronic stopping power. For protons and other ions, the Total Ionizing Dose (TID) is equal to the product of LET and fluence. For MeV and GeV charged particles, the two are essentially the same. Similarly, what is commonly termed the Non-Ionizing Energy Loss (NIEL) is the same thing as Nuclear Stopping Power used by ion implantation specialists.

The range and resulting ion distribution are calculated by a number of codes, one of the most common being Stopping and Range of Ions in Matter (SRIM) <sup>(109)</sup>. Figure 5 shows the calculated energy loss profiles for protons of 20 MeV or 1 GeV energy in  $\text{Ga}_2\text{O}_3$ . Note at these

energies, the protons will completely traverse the thickness of a normal Ga<sub>2</sub>O<sub>3</sub> substrate (~750 μm). The electronic and nuclear (NIEL) stopping powers of Ga<sub>2</sub>O<sub>3</sub> to protons up to 1 GeV energy are given in Figure 6. Note that the ionizing (electronic) energy loss is dominant over this entire range of energies. NIEL, often called Displacement Damage (DD) depends on the particle fluence  $\Phi$  (number of ions /cm<sup>2</sup>). The units of NIEL are (keV-cm<sup>2</sup>/g) and the DD dose is given by the product of NIEL  $\times \Phi$ .

Figure 7 shows the LET as a function of proton energy in Ga<sub>2</sub>O<sub>3</sub>, calculated from SRIM. Note how this falls rapidly with proton energy, which is the basis for the utility of protons being used to deliver energy to spatially limited locations within electronic devices. This is used in device isolation schemes and in irradiation of tumors while minimizing damage to areas around the tumor.

#### **(iv) Effects of Proton Irradiation of Ga<sub>2</sub>O<sub>3</sub>**

There are an increasing number of radiation-hardened components now made out of wide and ultra-wide bandgap semiconductors because it helps in reducing the size and weight and improves the computation speed. The global radiation-hardened electronics for space applications market is estimated to reach \$4.8 billion in 2032 from \$2.4 billion in 2021, at a growth rate of 1.70% during the forecast period. The growth in the global radiation-hardened electronics for space applications market is expected to be driven by increasing demand for communication and Earth observation satellites. Over the past few years, there has been a drastic shift toward adopting small satellites over conventional ones. Moreover, the market has been witnessing a drift in the trend from using small satellites for one-time stints toward their regular use in satellite constellations. With the rapid growth in small satellite constellations for various applications such as Earth observation, remote sensing, and space-based broadband services, the

demand for radiation-hardened electronic components has also significantly increased. Several projects are currently in progress to produce advanced radiation-hardened electronics with enhanced capability to shield space perturbations at low cost, which are expected to increase with the launch of upcoming mega-constellations as well as with the rising interest of companies in satellite components that can sustain in the harsh space environment for longer period of time. Changes in the diffusion length of a semiconductor are a sensitive indicator of the presence of radiation damage <sup>(110,111)</sup>. Electron Beam-Induced Current (EBIC) and Cathodoluminescence (CL) measurements can characterize the diffusion length (L) of minority carriers (electrons) and luminescence behavior of such samples, respectively. Nominally p-type Ga<sub>2</sub>O<sub>3</sub> samples were irradiated with protons having a dose/energy sequence to create a near-uniform hydrogen concentration around 10<sup>19</sup> cm<sup>-3</sup>. This consisted of 25 keV/1.6 x10<sup>14</sup> cm<sup>-2</sup>, 50 keV/1.7x10<sup>14</sup> cm<sup>-2</sup> and 70 keV/3.6x10<sup>14</sup> cm<sup>-2</sup>. The temperature dependence of L before and after proton irradiation is shown in Figure 8. Within the current temperature range of measurements, it is likely that the origin of L decrease is due to mobility degradation due to phonon scattering.

Figure 9 shows normalized room temperature CL spectra before and after proton irradiation and after subsequent electron injection from an electron beam. The initial creation of vacancies produces some reduction in strain-induced broadening, while there was no additional change after the electron injection, but the latter was accompanied by an increase in carrier lifetime, indicating athermal annealing of radiation defects.

#### **(v) Summary of Radiation Trap States and Carrier Removal Rates in β-Ga<sub>2</sub>O<sub>3</sub>**

Figure 10 summarizes report trap states for as-grown and irradiated β-Ga<sub>2</sub>O<sub>3</sub>. These include the position of these states in the bandgap and the possible identification of the origin of the traps. Note the importance of V<sub>Ga</sub> related states. After irradiation, it is observed that the

concentration of some of the defects present in the as-grown material increases, suggesting the contained vacancy-related defects to begin with <sup>(112-129)</sup>.

A summary of carrier removal rates is given in Figure 11 (top) for irradiated  $\beta$ -Ga<sub>2</sub>O<sub>3</sub>. The removal rates are highest for alpha particles, followed by protons, neutrons, electrons and gamma rays. This is in general agreement with the relative amount of NIEL associated with each type of radiation. Electron removal rates at low proton energies are usually much lower than predicted based on SRIM calculations of the Ga vacancies densities, presumably because of the dynamic annealing. For energies ~10-20 MeV experimental values are close to calculated. At very high proton energies the actual removal rates are higher than predicted.

The removal rates for  $\beta$ -Ga<sub>2</sub>O<sub>3</sub> for protons and neutrons are on par with those reported for GaN and SiC, as shown for the example of GaN and related alloys in Figure 11(bottom). Since the differences with Si would be less than a factor of 2 based purely on threshold energies for displacement, the presence of strong dynamic annealing in the wide bandgap semiconductors must be invoked and is consistent with the known diffusivity of primary point defects in these materials at and above room temperature.

#### **(vi) TCAD simulations of Heavy Ion Strikes and Preliminary Charge Collection-Experiments in $\beta$ -Ga<sub>2</sub>O<sub>3</sub>**

SiC and GaN power devices are susceptible to degradation from single event effects (SEE) resulting from the high-energy, heavy-ion space radiation environment (galactic cosmic rays) that cannot be shielded. This degradation occurs at < 50% of the rated operating voltage, requiring operation of SiC MOSFETs and rectifiers at de-rated voltages. SEE caused by terrestrial cosmic radiation (neutrons) have also been identified by industry as a limiting factor for the use of SiC-based electronics in aircraft. A single event effect occurs when a single heavy

ion or high-energy proton impacts a device. This ion will create a trail of hole and electron pairs which can be swept into the electric field of the device. A heavy ion strike can cause different kinds of effects, both non-destructive and destructive. The destructive single event effects are single event burnout (SEB), single event gate rupture (SEGR), and single event dielectric rupture (SEGR). SEB and SEGR are different mechanisms, but they can be hard to distinguish. SEB generally refers to what happens in a power MOSFET when ionization causes the breakdown voltage to be exceeded and the radiation-induced high current may cause catastrophic damage to the device. In other words, single-ion-induced strike causes a localized high-current state, which may result in catastrophic device failure, and is normally characterized by a significant increase in drain current that exceeds the device rating. However, basically nothing is known about SEE in Ga<sub>2</sub>O<sub>3</sub>.

We have performed some preliminary TCAD simulations of charge collection response to a heavy-ion strike and the resulting single event burnout on  $\beta$ -Ga<sub>2</sub>O<sub>3</sub> Schottky diodes with biased field rings<sup>(130)</sup>. The charge removal after simulated heavy-ion strikes was greatly improved with these field rings<sup>(123)</sup>. The breakdown of rectifiers occurs near the contact edge where the electric field is the highest during the voltage blocking operation and device failure is usually triggered here Figure 12 shows that when using concentric field rings, the current drops to zero faster, whereas with no rings there is a residual charge remaining at the contact edge Adding rings improves the charge removal, while the smaller spacing between rings also removes the charge faster. Both the position of the strike and the LET value influence the charge removal rate. An example is shown in Figure 13. These simulations clearly show that use of biased rings greatly improves both the breakdown voltage of the device and the charge removal after simulated heavy ion strikes, showing a pathway to use device design to partially mitigate single event effects in  $\beta$ -

Ga<sub>2</sub>O<sub>3</sub> power rectifiers. Some preliminary experimental data has also been generated by mapping the spatial dependence of laser-induced transient shapes. Location-specific changes in the shape of the transients and the amount of collected charge provide insight into trap formation and charge-collection mechanisms. A pulsed laser is used to generate spatial plots of SET amplitudes and collected charge, from which regions of enhanced SET signals, or “hot spots”, are identified. These hot spots are attributed to the presence of lattice defects that modify the local electric field, particularly in the source-drain, region near the edge of the gate where the transient sensitivity is greatest.

SEE are one-time events caused by a high-energy particle striking a device and resulting in an event, such as a current transient, an upset, a latch-up, or damage. A key parameter is the Linear Energy Transfer (LET), which is the amount of energy transferred per unit length as the ion travels through a material, expressed as MeV/(mg/cm<sup>2</sup>) or energy divided by density, the ion stopping power for a given target. The cross section is the number of errors produced in the device under test divided by the fluence, in units of cm<sup>2</sup>. The cross section gives a probability of a single event occurring. To simulate these effects, testing has traditionally been done with an accelerator. Many of the high-energy heavy ions and protons encountered in space typically cannot be shielded, so mitigation involves adding redundancy or reset circuitry. Prompt dose is also referred to as dose rate upset or dose rate latch-up and is caused by a flash of high energy photons from a nuclear explosion. This results in large photocurrents developing inside the devices or circuits. The dose rate here is many orders of magnitude higher than used for TID testing. The photocurrents can cause effects similar to single event effects, but multiple effects can occur at once.

Figure 14 shows an example of a charge collection waveform for laser irradiation of a Ga<sub>2</sub>O<sub>3</sub> rectifier, along with the collected charge as a function of laser energy. These fundamental studies will help elucidate charge collection dynamics in Ga<sub>2</sub>O<sub>3</sub> devices.

### **Summary and Conclusions**

While there has been significant progress in understanding radiation damage effects in Ga<sub>2</sub>O<sub>3</sub>, these are questions that need additional research:

- a) Is there a synergistic effect between total dose and SEE in Ga<sub>2</sub>O<sub>3</sub>, through increased off-state leakage due to cumulative ion strikes below disruption threshold?
- b) what is the effect of mixed radiation environments more typical of what Ga<sub>2</sub>O<sub>3</sub> avionics will encounter?
- c) what is the effect of temperature on SEE response in Ga<sub>2</sub>O<sub>3</sub>?
- d) what is the role of hydrogen, either in gate dielectrics or in forming defect-H complexes?  
(131-135)
- e) are there any Ga<sub>2</sub>O<sub>3</sub> device specifications (e.g., the electric field profile, contact metal) that act as “predictors” of more severe radiation effects?
- f) does electrical aging increase susceptibility to radiation-induced failure in Ga<sub>2</sub>O<sub>3</sub>?
- g) what are the threshold displacement energies for each type of radiation for Ga<sub>2</sub>O<sub>3</sub>?

### **Acknowledgments**

Work performed as part of Interaction of Ionizing Radiation with Matter University Research Alliance (IIRM-URA), sponsored by the Department of the Defense, Defense Threat Reduction Agency under award HDTRA1-20-2-0002. The content of the information does not necessarily reflect the position or the policy of the federal government, and no official endorsement should be inferred. AH also acknowledges support from the US National Science Foundation (ECCS #

2015795). The work at UF was also supported by NSF DMR 1856662 (James Edgar). The work at NRL was partially supported by the Office of Naval Research.

## References

1. S.J. Pearton, Y.- S. Hwang and F. Ren, *J. Mater.* **67**, 1359 (2015).
2. E. B. Yakimov, P. S. Vergeles, A. Y. Polyakov, I.-H. Lee, S. J. Pearton, *Appl. Phys. Lett.*, **106**, 132101 (2015).
3. B.D. Weaver, T.J. Anderson, A.D. Koehler, J.D. Greenlee, J.K. Hite, D.I. Shahin, F.J. Kub, K.D. Hobart, *ECS J. Solid State Sci. Technol.* **5**, Q208 (2016).
4. C. Schwartz, A. Yadav, M. Shatkin, E. Flitsiyan, L. Chernyak, V. Kasiyan, L. Liu, Y. Xi, F. Ren and S.J. Pearton, *Appl. Phys. Lett.* **102**, 062102 (2013).
5. In Hwan Lee, A.Y. Polyakov, E.B. Yakimov, N.B. Smirnov, I.V. Shchemerov, S.A. Tarelkin, S.I. Didenko, K.I. Tapero, R.A. Zinovyev and S.J. Pearton, *Appl. Phys. Lett.* **110**, 112102 (2017).
6. Shihyun Ahn, ByungJae Kim, Yi Hsuan Lin, Fan Ren, S. J. Pearton, Gwangseok Yang, Jihyun Kim and Ivan Kravchenko, *J. Vac. Sci. Technol. B* **34**, 051202 (2016).
7. B.J. Kim, S. Ahn, Fan Ren, S. J. Pearton, G. Yang and J. Kim, *J. Vac. Sci. Technol. B* **34**, 041231(2016).
8. Ya Shi Hwang, Lu Liu, F. Ren, A.Y. Polyakov, N. B. Smirnov, A. V. Govorkov, E. A. Kozhukhov, N.G. Kolin, V. M. Boiko, S S Vereyovkin, V Ermakov, C. F. Lo, O.A. Laboutin, Yu Cao, J. W. Johnson, N. I. Kargin, R. V. Ryzhuk and S.J. Pearton, *J. Vac. Sci. Technol. B* **31**, 022206 (2013).
9. L. Liu, C. V. Cuervo, Y. Xi, F. Ren, S. J. Pearton, H.Y. Kim, J. Kim and I. I. Kravchenko, *J. Vac. Sci. Technol. B* **31**, 042202 (2013).
10. E. Patrick, M. Choudhury, F. Ren, S.J. Pearton and M.E. Law, *ECS J. Solid State Sci. Technol.* **4**, Q21 (2015).

11. L. Chernyak, A. Yadav, E. Flitsiyan, Y.-H. Hwang, Y.-L. Hsieh, L. Lei, F. Ren and S. J. Pearton, *Rad. Effects and Defects in Solids*, **170**, 234 (2015).
12. J.D. Greenlee, P. Specht, T.J. Anderson, A.D. Koehler, B.D. Weaver, Martina Luysberg, Oscar D. Dubon, Francis J. Kub, Todd R. Weatherford, Karl D. Hobart, *Appl. Phys. Lett.* **107**, 083504 (2015)
13. T. Anderson, A. Koehler, Y.-H. Hwang, Y.-L. Hsieh, S. Li, Fan Ren, J. W. Johnson and S. J. Pearton, *J. Vac. Sci. Technol. B* **32**, 051203 (2014).
14. L. Liu, Y.-H. Hwang, Y. Xi, F. Ren, V. Craciun, S.J. Pearton, G. Yang, H.- Y. Kim and J. Kim, *J. Vac. Sci. Technol. B.* **32**, 022202 (2014).
15. Andrew D. Koehler, Travis J. Anderson, Marko J. Tadjer, Bradley D. Weaver, Jordan D. Greenlee, David I. Shahin, Karl D. Hobart, Francis J. Kub, *IEEE Electron Dev. Lett.* **37**, 545 (2016).
16. Y.S. Puzyrev, T. Roy, E.X. Zhang, D.M. Fleetwood, R.D. Schrimpf, S.T. Pantelides, *IEEE Trans Nuclear Science*, **58**, 2918 (2011).
17. M. H. Wong and M. Higashiwaki, *IEEE Trans Electron Dev*, **67**, 3925 (2020).
18. Andrew J. Green, James Speck, Grace Xing, Peter Moens, Fredrik Allerstam, Krister Gumaelius, Thomas Neyer, Andrea Arias-Purdue, Vivek Mehrotra, Akito Kuramata, Kohei Sasaki, Shinya Watanabe, Kimiyoshi Koshi, John Blevins, Oliver Bierwagen, Sriram Krishnamoorthy, Kevin Leedy, Aaron R. Arehart, Adam T. Neal, Shin Mou, Steven A. Ringel, Avinash Kumar, Ankit Sharma, Krishnendu Ghosh, Uttam Singiseti, Wenshen Li, Kelson Chabak, Kyle Liddy, Ahmad Islam, Siddharth Rajan, Samuel Graham, Sukwon Choi, Zhe Cheng, and Masataka Higashiwaki, *APL Mater.* **10**, 029201 (2022).
19. S. J. Pearton, Fan Ren, Marko Tadjer and Jihyun Kim, *J. Appl. Phys.* **124**, 220901 (2018).

20. M. Bosi, P. Mazzolini, L. Seravalli and R. Fornari, *J. Mater. Chem. C*, **8**, 10975 (2020).
21. S. Roy, A. Bhattacharyya, P. Ranga, H. Splawn, J. Leach and S. Krishnamoorthy, *IEEE Electron Dev. Lett.* **42**, 1140 (2021).
22. X. Lu, X. Zhou, H. Jiang, K. W. Ng, Z. Chen, Y. Pei, K. M. Lau, and G. Wang, *IEEE Electron Dev Lett.* **41**, 449 (2020).
23. B. Chatterjee, K. Zeng, C. D. Nordquist, U. Singiseti and S. Choi, *IEEE Trans. Compon, Packaging Man Technol*, **9**, 2352 (2019).
24. K. D. Chabak, K. D. Leedy, A. J. Green, S. Mou, A. T Neal, T. Asel, E. R. Heller, N. S. Hendricks, K. Liddy, A. Crespo, N. C. Miller, M. T. Lindquist, N. Moser, R. C. Fitch Jr, D. E. Walker Jr, D. L Dorsey and G. H. Jessen, *Semicond Sci Technol*, **35**, 013002 (2020).
25. Wenshen Li, Devansh Saraswat, Yaoyao Long, Kazuki Nomoto, Debdeep Jena, and Huili Grace Xing, *Appl. Phys. Lett.* **116**, 192101 (2020)
26. Y. Lv, Y. Wang, X. Fu , Shaobo Dun, Z. Sun, Hongyu Liu, X. Zhou, X. Song, K. Dang, S. Liang, J. Zhang, H. Zhou, Z. Feng, S. Cai and Yue Hao, *IEEE Trans Power Electron.* **36**, 6179 (2021).
27. Jiancheng Yang, Minghan Xian, Patrick Carey, Chaker Fares, Jessica Partain, Fan Ren, Marko Tadjer, Elaf Anber, Dan Foley, Andrew Lang, James Hart, James Nathaniel, Mitra L. Taheri, S. J. Pearton and Akito Kuramata, *Appl. Phys. Lett.* **114**, 232106 (2019)
28. Z. Jian, S. Mohanty and E. Ahmadi, *Appl. Phys. Lett.*, **116**, 152104 (2020).
29. J. Yang, F. Ren, Y.-T. Chen, Y.-T. Liao, C.-W. Chang, J. Lin, M. J.Tadjer, S. J. Pearton, and A. Kuramata, *IEEE J. Electron Dev. Soc.*, **7**, 57 (2019).
30. W. Xiong, X. Zhou, G. Xu, Q. He, G. Jian, C. Chen, Y. Yu, W. Hao, X. Xiang, X. Zhao, W. Mu, Z. Jia, X. Tao, and S. Long, *IEEE Electron. Dev. Lett.***42**, 430 (2021).

31. Chenlu Wang, Hehe Gong, Weina Lei, Y. Cai, Z. Hu, Shengrui Xu, Zhihong Liu , Qian Feng , Hong Zhou, Jiandong Ye, Jincheng Zhang, Rong Zhang, and Yue Hao, *IEEE Electron Dev. Lett.*, **42**, 485 (2021).
32. S. Roy, A. Bhattacharyya, P. Ranga, H. Splawn, J. Leach, and S. Krishnamoorthy, *IEEE Electron Device Lett.*, **42**, 1540 (2021).
33. Qinglong Yan, Hehe Gong, Jincheng Zhang, Jiandong Ye, Hong Zhou, Zhihong Liu, Shengrui Xu, Chenlu Wang, Zhuangzhuang Hu, Qian Feng, Jing Ning, Chunfu Zhang, Peijun Ma, Rong Zhang, and Yue Hao, *Appl. Phys. Lett.* **118**, 122102 (2021).
34. H. H. Gong, X. H. Chen, Y. Xu, F.-F. Ren, S. L. Gu and J. D. Ye, *Appl. Phys. Lett.*, **117**, 022104 (2020).
35. W. Hao, Q. He, K. Zhou, G. Xu, W. Xiong, X. Zhou, G. Jian, C. Chen, X. Zhao, and S. Long, *Appl. Phys. Lett.*, **118**, 043501 (2021).
36. F. Zhou, Hehe Gong, Weizong Xu, Xinxin Yu, Yang Xu, Yi Yang, Fang-fang Ren, Shulin Gu, Youdou Zheng, Rong Zhang, Jiandong Ye and Hai Lu, *IEEE Trans. Power Electron.*, **37**, 1223 (2022)
37. Qinglong Yan, Hehe Gong, Jincheng Zhang, Jiandong Ye, Hong Zhou, Zhihong Liu, Shengrui Xu, Chenlu Wang, Zhuangzhuang Hu, Qian Feng, Jing Ning, Chunfu Zhang, Peijun Ma, Rong Zhang, and Yue Hao, *Appl. Phys. Lett.* **118**, 122102 (2021).
38. Qinglong Yan, Hehe Gong, Hong Zhou, Jincheng Zhang, Jiandong Ye, Zhihong Liu, Chenlu Wang, Xuefeng Zheng, Rong Zhang, and Yue Hao, *Appl. Phys. Lett.* **120**, 092106 (2022).

39. Y. J. Lv, Y. G. Wang, X. C. Fu, S. B. Dun, Z. F. Sun, H. Y. Liu, X. Y. Zhou, X. B. Song, K. Dang, S. X. Liang, J. C. Zhang, H. Zhou, Z. H. Feng, S. J. Cai, and Y. Hao, *IEEE Trans. Power Electron.* **36**, 6179 (2021).
40. Yuangang Wang, Hehe Gong, Yuanjie Lv, Xingchang Fu, Shaobo Dun, Tingting Han, Hongyu Liu, Xingye Zhou, Shixiong Liang, Jiandong Ye, Rong Zhang, Aimin Bu, Shujun Cai and Zhihong Feng, *IEEE Trans. Power Electron.* **37**, 3743 (2022).
41. S. J. Pearton, J. Yang, P. H. Cary, F. Ren, J. Kim, M. J. Tadjer, and M.A. Mastro, *Appl. Phys. Rev.*, **5**, 011301 (2018).
42. S. J. Pearton, Assel Aitkaliyeva, Minghan Xia, Fan Ren, Ani Khachatryan, Adrian Ildefonso, Zahabul Islam, Md Abu Jafar Rasel, Aman Haque, A. Y. Polyakov and Jihyun Kim, *ECS J. Solid. State Sci. Technol.* **10**, 055008 (2021).
43. See <https://www.novelcrystal.co.jp/eng/archives/911> for information about gallium oxide vertical transistor with highest breakdown voltage.
44. Ribhu Sharma, Minghan Xian, Chaker Fares, Mark E. Law, Marko Tadjer, Karl D. Hobart, Fan Ren, Stephen J. Pearton, *J. Vacuum Sci. Technology A*, **39**, 013406 (2021).
45. S. Kuboyama, C. Kamezawa, N. Ikeda, T. Hirao, and H. Ohyama, *IEEE Trans. Nucl. Sci.*, **53**, 3343 (2006).
46. S. Kuboyama, C. Kamezawa, Y. Satoh, T. Hirao and H. Ohyama, *IEEE Trans. Nucl. Sci.*, **54**, 2379 (2007).
47. T. Makino, M. Deki, N. Iwamoto, S. Onoda, N. Hoshino, H. Tsuchida, T. Hirao and T. Ohshima, *IEEE Trans. Nucl. Sci.*, **60**, 2647 (2013).
48. S. Kuboyama, *IEEE Trans. Nucl. Sci.* **66**, 688 (2019).
49. H. Xue, Y. Zhang, W.J. Weber, *Materials Research Letters* **5**, 494 (2017)

50. J.-M. Lauenstein, *Getting SiC Power Devices Off the Ground: Design, Testing, and Overcoming Radiation Threats*, Microelectronics Reliability and Qualification Working (MRQW) Meeting, El Segundo, CA, February 2018.  
<https://ntrs.nasa.gov/search.jsp?R=20180006113>
51. L. B. Bayu Aji, J. B. Wallace and S. O. Kucheyev, *Scientific Reports* **7**, 44703 (2017).
52. E. Mizuta, S. Kuboyama, H. Abe, Y. Iwata and T. Tamura, *IEEE Trans. Nuclear Sci*, **61**,1924 (2014).
53. Ki-Man Lee, Byung-Gun Park, *IEEE Trans. Nuclear Sci*, **67**, 1374 (2020).
54. R. D. Harris, A. J. Frasca and M. O. Patton, *IEEE Trans Nuclear Sci.*, **52**, 2408 (2005).
55. P. Hazdra, P. Smrkovský, J. Vobecký and A. Mihaila, *IEEE Trans Electron Dev.* **68**, 202 (2021)
56. D.R. Ball, B.D. Sierawski, K.F. Galloway, R.A. Johnson, M.L. Alles, A.L. Sternberg, A.F. Witulski, R.A. Reed, R.D. Schrimpf, Arto Javanainen, J-M. Lauenstein, *IEEE Trans. Nuclear Sci* **66**, 337 (2018)
57. Joel M. Hales, Nicolas J-H. Roche, Ani Khachatryan, Dale Mcmorrow, Stephen Buchne, Jeffrey Warner, Marek Turowski, Klas Lilja, Nicholas C. Hooten, En Xia Zhang, Robert A. Reed, Ronald D. Schrimpf, *IEEE Trans Nuclear Sci*, **64**, 1006 (2017)
58. K.F. Galloway, A.F. Witulski, R.D. Schrimpf, A.L. Sternberg, D.R. Ball, Dennis R. Ball, Arto Javanainen, Robert A. Reed, Brian D. Sierawski, Jean-Marie Lauenstein, *Aerospace*, **5** (3), 67 (2018).
59. D. R. Ball, K. F. Galloway, R. A. Johnson, M. L. Alles, A. L. Sternberg, B. D. Sierawski, A. F. Witulski, R. A. Reed, R. D. Schrimpf, J. M. Hutson, A. Javanainen, J.-M. Lauenstein, *IEEE Trans. Nucl. Sci*, **67**, 22 (2020).

60. Arto Javanainen, Marek Turowski, Kenneth F Galloway, Christopher Nicklaw, Véronique Ferlet-Cavrois, Alexandre Bossier, Jean-Marie Lauenstein, Michele Muschitiello, Francesco Pintacuda, Robert A. Reed, Ronald D. Schrimpf, Robert A Weller, Ari Virtanen, *IEEE Trans. Nucl. Sci.*, **64**, 2031 (2017).
61. Xin-Xing Fei, Ying Wang, Xin Luo, Meng-Tian Bao, Cheng-Hao Yu, Xing-Ji Li, *Microelectron Rel.*, **110**, 113699 (2020).
62. C. Abbate, G. Busatto, P. Cova, N. Delmonte, F. Giuliani, F. Iannuzzo, A. Sanseverino, and F. Velardi, *IEEE Trans. Nucl. Sci.* **62**, 202 (2015).
63. J. A. McPherson, P. J. Kowal, G. K. Pandey, T. P. Chow, W. Ji, and A. A. Woodworth, *IEEE Trans. Nucl. Sci.* **66**, 474 (2019).
64. A. Akturk, R. Wilkins, J. McGarrity, and B. Gersey, *IEEE Trans. Nucl. Sci.*, **64**, 529 (2017).
65. J.-M. Lauenstein, M. C. Casey, and K. A. LaBel, “Single-event effects in silicon and silicon carbide power devices,” in Proc. NASA NEPP Electron. Technol. Workshop, Jun. 2014, pp. 1–18.. <https://ntrs.nasa.gov/api/citations/20140017356/downloads/20140017356.pdf>
66. D. R. Ball, K. F. Galloway, R. A. Johnson, M. L. Alles, A. L. Sternberg, A. F. Witulski, R. A. Reed, R. D. Schrimpf, J. M. Hutson and J.-M. Lauenstein, *IEEE Trans Nucl. Sci.*. **68**, 1430 (2021).
67. J.M. Lauenstein, 2021 NEPP Electronics Technology Workshop, Greenbelt, MD, June 14-17, 2021
68. S.J. Pearton, Aman Haque, Ani Khachatryan, Adrian Ildefonso, Leonid Chernyak and Fan Ren, *ECS J. Solid State Sci. Technol.* **10**, 075004 (2021).

69. A.Y. Polyakov, N.B. Smirnov, I.V. Shchemerov, A.A. Vasilev, A.I. Kochkova, A.V.Chernykh, P.B. Lagov, Yu.S. Pavlov, V. S. Stolbunov, T.V. Kulevoy, I. V. Borzykh, In Hwan Lee, Fan Ren and S.J. Pearton, *J. Appl. Phys.* **130**, 035701 (2021).
70. E.B. Yakimov, A.Y. Polyakov, I.V. Shchemerov, N.B. Smirnov, A.A. Vasilev, P.S. Vergeles, E.E. Yakimov, A.V. Chernykh, F. Ren and S.J. Pearton, *Appl. Phys. Lett.* **118**, 202106 (2021).
71. A.Y. Polyakov, V.I. Nikolaev, E. B. Yakimov, F. Ren, S. J. Pearton, Jihyun Kim, *J. Vac. Sci. Technol. A* **40**, 020804 (2022).
72. A.Y. Polyakov, I.V. Shchemerov, A.A. Vasilev, A.I. Kochkova , N.B. Smirnov, A.V. Chernykh, E.B. Yakimov, P.B. Lagov, Yu.S. Pavlov, E.M. Ivanov, O.G. Gorbatkova, A.S. Drenin, M.E. Letovaltseva, Minghan Xian, Fan Ren, Jihyun Kim and S.J. Pearton, *J. Appl. Phys.* **130**, 185701 (2021).
73. M. Zerarka, P. Austin, A. Bensoussan, F. Morancho and A. Durier, *IEEE Trans. Nucl. Sci.* **64**, 2242 (2017).
74. R. Lingaparthi, Kohei Sasaki, Quang Tu Thieu, Akio Takatsuka, Fumio Otsuka, S. Yamakoshi and Akito Kuramata, *Appl. Phys. Expr.*, **12**, 074008 (2019).
75. United States Space Force, *Space Power*, Space Capstone Publication, June 2020
76. N.A. Theodoropoulou, A.F. Hebard, D.P. Norton, J.D. Budai and L.A. Boatner, *Solid-State Electron.* **47**, 2231 (2003).
77. J.C. Zolper, H.H. Tan, J.S. Williams, J. Zou, D.J.H. Cockayne and S.J. Pearton, *Appl. Phys. Lett.* **70**, 2729 (1997).
78. S. J. Pearton, C.R. Abernathy, M.B. Panish, R.A. Hamm and L.M. Lunardi, *J. Appl. Phys.* **66**, 656 (1989).

79. J.S. Lee, J.D. Lim, Z.G. Khim, Y.D. Park, S.J. Pearton and S.N.G. Chu, *J. Appl. Phys.* **93**, 4512 (2003).
80. K. Ip, M.E. Overberg, Y.W. Heo, D.P. Norton, S.J. Pearton and S.O. Kucheyev, *Appl. Phys. Lett.* **81**, 3996 (2002).
81. E.B. Yakimov, A.Y. Polyakov, I.V. Shchemerov, N.B. Smirnov, A.A. Vasilev, P.S. Vergeles, E.E. Yakimov, A.V. Chernykh, A. S. Shikoh, F. Ren and S.J. Pearton, *Appl. Phys. Mater.* **8**, 111105 (2020).
82. Sushrut Modak, Leonid Chernyak, Sergey Khodorov, Igor Lubomirsky, Arie Ruzin, Minghan Xian, Fan Ren and Stephen J. Pearton, *ECS J. Solid State Sci. Technol.* **9**, 045018 (2020).
83. Sushrut Modak, Leonid Chernyak, Sergey Khodorov, Igor Lubomirsky, Jiancheng Yang, Fan Ren and S. J. Pearton, *ECS J. Solid State Sci. Technol.* **8**, Q3050 (2019).
84. J. C. Yang, Gregory J. Koller, Chaker Fares, F. Ren, S. J. Pearton, Jinho Bae and Jihyun Kim, *ECS J. Solid State Sci. Technol.* **8**, Q3041 (2019).
85. A.Y. Polyakov, N.B. Smirnov, I.V. Shchemerov, A. A. Vasilev, E. B. Yakimov, A. V. Chernykh, A.I. Kochkova, P. B. Lagov, Yu. S. Pavlov, O.F. Kukharchuk, A.A. Suvorov, N.S. Garanin, In Hwan Lee, Minghan Xian, Fan Ren and S.J. Pearton, *J. Phys. D* **53**, 274001 (2020).
86. M. Xian, Chaker Fares, Jinho Bae, Jihyun Kim, Fan Ren and S.J. Pearton, *ECS J. Solid State Sci. Technol.* **8**, P799 (2019).
87. A.Y. Polyakov, N. B. Smirnov, I Shchemerov, S. J. Pearton, Fan Ren, A. Chernykh, P.B. Lagov and Timur V. Kulevoy, *APL. Mater.* **6**, 096102 (2019).
88. Jiancheng Yang, Chaker Fares, Yu Guan, F. Ren, S. J. Pearton, Jinho Bae, Jihyun Kim and Akito Kuramata, *J. Vac. Sci. Technol. B.* **36**, 031205 (2018).

89. J. D. Lee, Elena Flitsiyan, Leonid Chernyak, Jiancheng Yang, Fan Ren, S. J. Pearton, Boris Meyler and Y. Joseph Salzman, *Appl. Phys. Lett.* **112**, 082104 (2018).
90. M. E. Ingebrigtsen, A. Yu. Kuznetsov, B. G. Svensson, G. Alfieri, A. Mihaila, U. Badstübner, A. Perron, L. Vines, and J. B. Varley, *APL Materials* **7**, 022510 (2019).
91. B. E. Kananen, L. E. Halliburton, K. T. Stevens, G. K. Foundos, K. B. Chang, and N. C. Giles, *Appl. Phys. Lett.* **110**, 202104 (2017).
92. Filip Tuomisto, Antti Karjalainen, Vera Prozheeva, Ilja Makkonen, Gunter Wagner, Michele Baldini, Oxide-based Materials and Devices X, edited by David J. Rogers, David C. Look, Ferechteh H. Teherani, *Proc. Of SPIE* Vol. **10919**, 1091910 (2020)
93. E. Korhonen, F. Tuomisto, D. Gogova, G. Wagner, M. Baldini, Z. Galazka, R. Schewski and M. Albrecht, *Appl. Phys. Lett.* **106**, 242103 (2015).
94. Philip Weiser, Michael Stavola, W. Beall Fowler, Ying Qin and S.J. Pearton, *Appl. Phys. Lett.* **112**, 232104 (2018).
95. M.H. Wong, A. Takeyama, T. Makino, T. Ohshima, K Sasaki, A. Kuramata, S. Yamakoshi and M. Higashiwaki, *Appl. Phys. Lett.* **112**, 023503 (2018).
96. J. Yang, F. Ren, S.J. Pearton, G. Yang, J. Kim and A. Kuramata, *J. Vac. Sci. Technol. B* **35**, 031208 (2017).
97. A.Y. Polyakov, N.B. Smirnov, I.V. Shchemerov, E.B. Yakimov, Jiancheng Yang, F. Ren, Gwangseok Yang, Ji Hyun Kim, A. Kuramata and S. J. Pearton, *Appl. Phys. Lett.* **112**, 032107 (2018).
98. G. Yang, S. Jang, F. Ren, S.J. Pearton and J. Kim, *ACS Appl. Mater. Interfaces* **9**, 40471 (2017).

99. J. Yang, Zhiting Chen, F. Ren, S. J. Pearton, Gwangseok Yang, Jihyun Kim, Jonathan Lee, Elena Flitsiyan and Leonid Chernyak and A. Kuramata, *J. Vac. Sci. Technol. B* **36**, 011206 (2018).
100. J. C. Yang, F. Ren, R. Khanna, K. Bevlín, D. Geerpuram, Li-Chun Tung, Jingyu Lin and Hongxing Jiang, Jonathan Lee, Elena Flitsiyan, Leonid Chernyak, S. J. Pearton and A. Kuramata, *J. Vac. Sci. Technol. B* **35**, 051201 (2017).
101. A.Y. Polyakov, N.B. Smirnov, I.V. Shchemerov, E.B. Yakimov, S.J. Pearton, Chaker Fares, Jiancheng Yang, Fan Ren, Jihyun Kim, P.B. Lagov, V. S. Stolbunov, and A. Kochkova, *Appl. Phys. Lett.* **113**, 092102 (2018).
102. M. E. Law and S. M. Cea, *Comput. Mater. Sci.* **12**, 289 (1998).
103. J. Kim, Stephen J. Pearton, Chaker Fares, Jiancheng Yang, Fan Ren, Suhyun Kim and Alexander Y. Polyakov, *J. Mater. Chem. C*, **7**, 10 (2019).
104. Md Abu Jafar Rasel, Sergei Stepanoff, Max Wetherington, Aman Haque, Douglas E. Wolfe, Fan Ren and Stephen Pearton, *Appl. Phys. Lett.* **120**, 124101 (2022).
105. Zahabul Islam, Angela L. Paoletta, Anthony M. Monterrosa, Jennifer D. Schuler, Timothy J. Rupert, Khalid Hattar, Nicholas Glavin, Aman Haque, *Microelectronics Rel.*, **102**, 113493 (2019).
106. T.-Huong Dang, M. Konczykowski, H. Jaffrès, V. I. Safarov, and H.-J. Drouhin, *J. Vac. Sci. Technol. A* **40**, 033416 (2022).
107. O. S. Oen, “Cross sections for atomic displacements in solids by fast electrons,” Technical Report, Office of Scientific and Technical Information (OSTI), ID No. 4457758, Report No. ORNL-4897, 1973.

108. P. Bois, “*Etude des défauts ponctuels dans le bismuth*,” CEA Report No. R-5389  
1987. See: <https://inis.iaea.org/collection/NCLCollectionStore/Public/18/082/18082185.pdf>
109. J. Ziegler, J.P. Biersack, M.D. Ziegler, *SRIM-The Stopping and Ranges of Ions in Solids* (SRIM Co., Chester, 2008); [www.srim.org](http://www.srim.org)
110. Sushrut Modak, Leonid Chernyak, Alfons Schulte, Minghan Xian, Fan Ren, S. J. Pearton, Arie Ruzi, Sergey S. Kosolobov, Vladimir P. Drachev, *AIP Advances*, **11**, 125014 (2021).
111. Sushrut Modak, Leonid Chernyak, Alfons Schulte, Corinne Sartel, Vincent Sallet, Yves Dumont, Ekaterine Chikoidze, Xinyi Xia, Fan Ren, Stephen J. Pearton, Arie Ruzin, Denis M. Zhigunov, Sergey S. Kosolobov, Vladimir P. Drachev, *APL Mater.* **10**, 031106 (2022).
112. Baoming Wang, Zahabul Islam, Aman Haque, Kelson Chabak, Michael Snure, Eric Heller and Nicholas Glavin, *Nanotechnol.* **29**, 31LT01(2018).
113. J. S. George, R. Koga, R. M. Moision, and A. Arroyo, “Single Event Burnout Observed in Schottky Diodes,” *2013 IEEE Radiation Effects Data Workshop (REDW)*, Jul. 2013, pp. 1–8.
114. A. F. Witulski, R. Arslanbekov, A. Raman, R. D. Schrimpf, A. L. Sternberg, K. F. Galloway, A. Javanainen, D. Grider, D. J. Lichtenwalner and B. Hull, *IEEE Trans. Nucl. Sci.* **65**, 256 (2018).
115. S. Kuboyama, Satoshi Kuboyama, Eiichi Mizuta, Yuki Nakada, Hiroyuki Shindou, Alain Michez, Jérôme Boch, Frédéric Saigné and Antoine Touboul, *IEEE Trans. Nucl. Sci.* **66**, 1688 (2019).
116. D. Hu, Helong Zhang, Xintian Zhou, Yunpeng Jia, Yu Wu, Xinyu Li, Yun Tang, “A Simulation Study on Single-Event Burnout in Power Normally-off AlGaIn/GaN HEMT,” in *2019 3rd International Conference on Electronic Information Technology and Computer Engineering (EITCE)*, Oct. 2019, pp. 1546–1549.

117. X.-X. Fei, Y. Wang, X. Luo, M.-T. Bao, C.-H. Yu, and X.-J. Li, *Microelectronics Rel.* **110**, 113699 (2020).
118. Y. Wang, Xin-Xing Fei, Xue Wu, Xingji Li, Jianqun Yan, Mengtian Bao, Fei Cao, *IEEE Trans. Electron Dev.* **67**, 5466 (2020).
119. M. Zerarka, P. Austin, A. Bensoussan, F. Morancho, and A. Durier, *IEEE Trans. Nucl. Sci.* **64**, 2242 (2017).
120. R. Sharma, M. Xian, M. E. Law, M. Tadjer, F. Ren, and S. J. Pearton, *J. Vac. Sci. Technol. A*, **38**, 063414 (2020).
121. M. Labeled, Nouredine Sengouga, Afak Meftah, Mohamed Labeled, Sinsu Kyoung, Hojoong Kim and You Seung Rim, *ECS J. Sol. State Sci. Technol.*, **9**, 125001 (2020).
122. J. Park and S.-M. Hong, *ECS J. Solid State Sci. Technol.* **8**, Q3116 (2019).
123. A. Khachatryan, N. J. H. Roche, D. McMorrow, J. H. Warner, S. P. Buchner and J. S. Melinger, *IEEE Trans. Nucl. Sci.* **61**, 3416 (2014).
124. J. M. Hales, Ani Khachatryan, Stephen Buchner, Nicolas J.-H. Roche, Jeffrey Warner, Zachary E. Fleetwood, Adrian Ildefonso, John D. Cressler, Veronique Ferlet-Cavrois, and Dale McMorrow, *IEEE Trans. Nucl. Sci.* **65**, 1724 (2018).
125. J. M. Hales, Nicolas J.-H. Roche, Ani Khachatryan, Dale McMorrow, Stephen Buchner, Jeffrey Warner, Marek Turowski, Klas Lilja, Nicholas C. Hooten, En Xia Zhang, Robert A. Reed and Ronald D. Schrimpf, *IEEE Trans. Nucl. Sci.* **62**, 2867 (2015).
126. A. Khachatryan N. J.-H. Roche, S. Buchner, A. D. Koehler, T. J. Anderson, V. Ferlet-Cavrois, M. Muschitiello, D. McMorrow, B. Weaver, and K. D. Hobart, *IEEE Trans. Nucl. Sci.* **62**, 2743 (2015).

127. J. M. Hales, A. Khachatryan, S. Buchner, N. J. Roche, J. Warner and D. McMorrow, *IEEE Trans. Nucl. Sci.* **64**, 1006 (2017).
128. A. Khachatryan, Nicolas J-H. Roche, Stephen P. Buchner, Andrew D. Koehler, Jordan D. Greenlee, Travis J. Anderson, Jeffrey H. Warner and Dale McMorrow, *IEEE Trans. Nucl. Sci.* **63**, 1995 (2016).
129. L. D. Ryder, Kaitlyn L. Ryder, Andrew L. Sternberg, John A. Kozub, Ani Khachatryan, Steven P. Buchner, Dale McMorrow, Joel M. Hales, Yuanfu Zhao, Liang Wang, Chuanmin Wang, Robert A. Weller, Ronald D. Schrimpf, Sharon M. Weiss and Robert A. Reed, *IEEE Trans. Nucl. Sci.* **68**, 2496 (2021).
130. Ribhu Sharma, Jian-Sian Li, Mark E. Law, Fan Ren and Stephen J. Pearton, presented at *2022 IEEE Nuclear and Space Radiation Effects Conf.*, July 18-22, 2022, Provo, Utah
131. Sushrut Modak, Alfons Schulte, Corinne Sartel, Vincent Sallet, Yves Dumont, Ekaterine Chikoidze Xinyi Xia, Fan Ren, Stephen J. Pearton, Arie Ruzin and Leonid Chernyak, *Appl. Phys. Lett.* **120**, 233503 (2022).
132. Andrew Venzie, Amanda Portoff, W. Beall Fowler, Michael Stavola, Dae Woo Jeon, Jihyun Kim and S. J. Pearton, *Appl. Phys. Lett.* **120**, 192101 (2022).
133. S.J. Pearton, S. Oh, S. Kim, Jihyun Kim and F. Ren, *Science Talks* **1**, 100001 (2022).
134. Md Abu Jafar Rasel, Sergei Stepanoff, Max Wetherington, Aman Haque, Douglas E. Wolfe, Fan Ren and Stephen Pearton, *Appl. Phys. Lett.* **120**, 124101 (2022).
135. Andrew Venzie, A. Portoff, E. Celeste Perez Valenzuela, Michael Stavola, W. B. Fowler, S. J. Pearton, and Evan R. Glaser, *J. Appl. Phys.* **131**, 035706 (2022).

## Figure Captions

Figure 1. Lattice structure of the three main polytypes for Ga<sub>2</sub>O<sub>3</sub>.

Figure 2. Schematic of vertical Ga<sub>2</sub>O<sub>3</sub> rectifier structure used for radiation studies.

Figure 3. Schematic of two main mechanisms by which Ga<sub>2</sub>O<sub>3</sub> degrades upon irradiation-removal of carriers to traps and reduction of carrier mobility by introduction of additional charged defects.

Figure 4. Calculated cross-section for electrons with Ga or O atoms in Ga<sub>2</sub>O<sub>3</sub>, as a function of electron energy.

Figure 5. Energy loss profiles for protons of 20 MeV or 1 GeV energy in Ga<sub>2</sub>O<sub>3</sub>, calculated from SRIM.

Figure 6. Electronic and nuclear stopping powers for <sup>1</sup>H<sup>+</sup> over a broad energy range in Ga<sub>2</sub>O<sub>3</sub> calculated from SRIM.

Figure 7. LET for Ga<sub>2</sub>O<sub>3</sub> with <sup>1</sup>H as a function of energy. The LET is the surface value due to ionization loss in the SRIM simulations.

Figure 8. Temperature dependence of diffusion length in lightly p-type Ga<sub>2</sub>O<sub>3</sub> before and after irradiation with protons at a cumulative dose of  $\sim 7 \times 10^{14}$  cm<sup>-2</sup>.

Figure 9. Normalized room-temperature cathodoluminescence spectrum (top) before and (center) after proton irradiation. A slight blue shift of the irradiation peak with smaller full width at half-maxima was observed after irradiation. After subsequent electron injection for 20 min (bottom) there is evidence of athermal defect annealing.

Figure 10. Compilation of reported trap states for as-grown and irradiated  $\beta$ -Ga<sub>2</sub>O<sub>3</sub>.

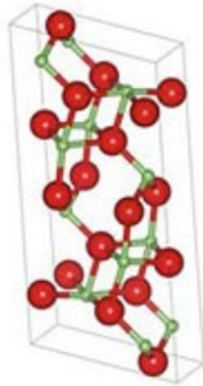
Figure 11. Summary of carrier removal rates for irradiated (top)  $\beta$ -Ga<sub>2</sub>O<sub>3</sub> and (bottom) GaN.

Figure 12. Hole concentrations in the device with (top) one concentric field ring as a function of time starting from  $10^{-13}$  (ion-strike) to  $10^{-6}$  s. The device with 1 ring is faster at charge removal compared to a (bottom) device without rings.

Figure 13. Simulated transient response to a heavy-ion strike at various positions in a rectifier structure, with two concentric field rings, a depth of ion strike of 4 $\mu$ m and ratio of bias applied on outermost ring contact to next inner contact  $V_r/V_g=0.95$ .

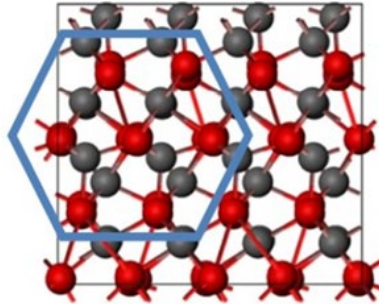
Figure 14. (top) Single event transient waveform for 250 pJ laser irradiation at 350nm, with the rectifier biased at 40V (bottom) collected charge as a function of 350 nm laser energy. Laser charge deposition takes place via two-photon absorption process.

**$\beta$**   
stable



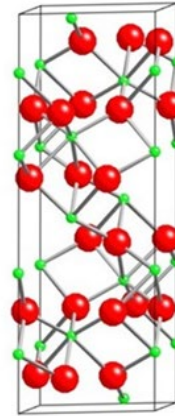
**Monoclinic**  
 **$\beta$ -Gallia**

**$\epsilon$**   
metastable

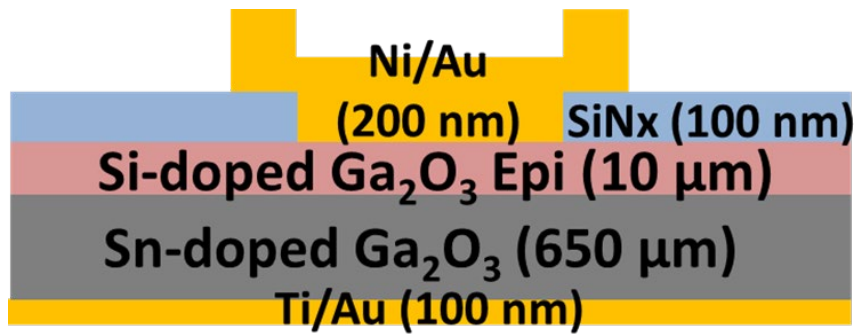


**Orthorhombic**  
 **$\kappa$ -Al<sub>2</sub>O<sub>3</sub>**

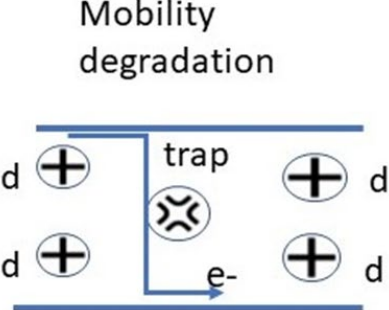
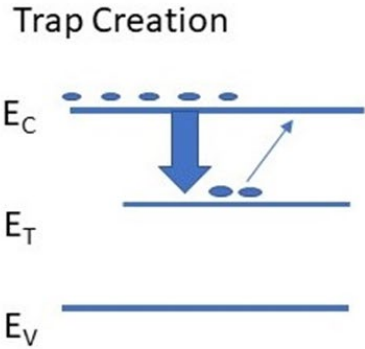
**$\alpha$**   
metastable

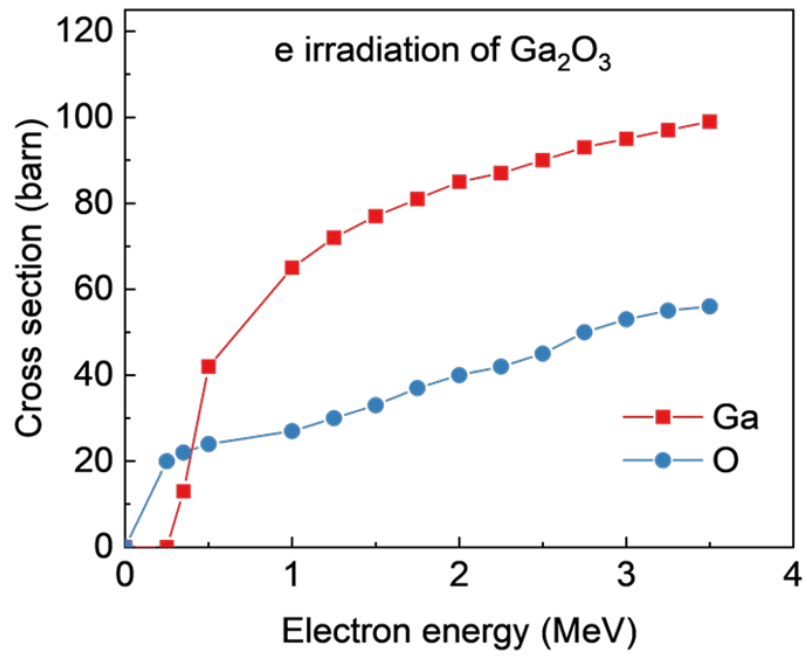


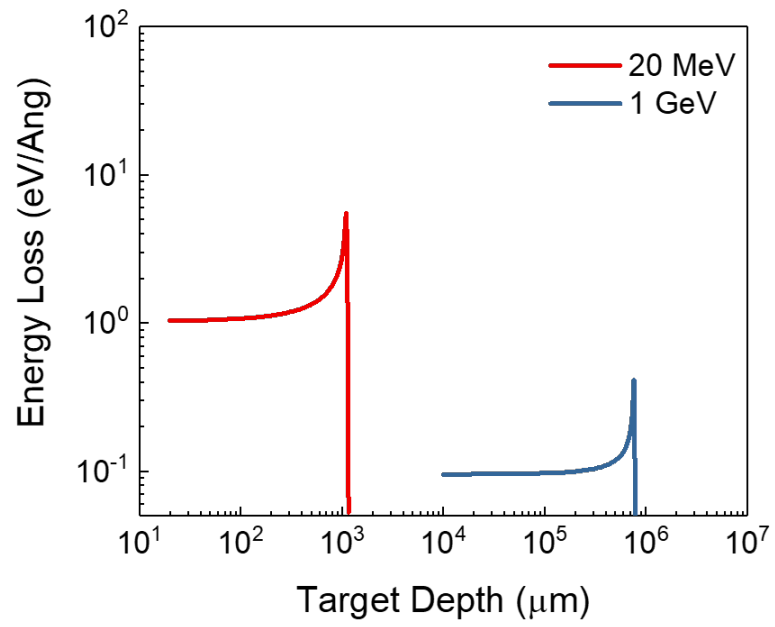
**Rhombohedral**  
**Corundum ( $\alpha$ -Al<sub>2</sub>O<sub>3</sub>)**

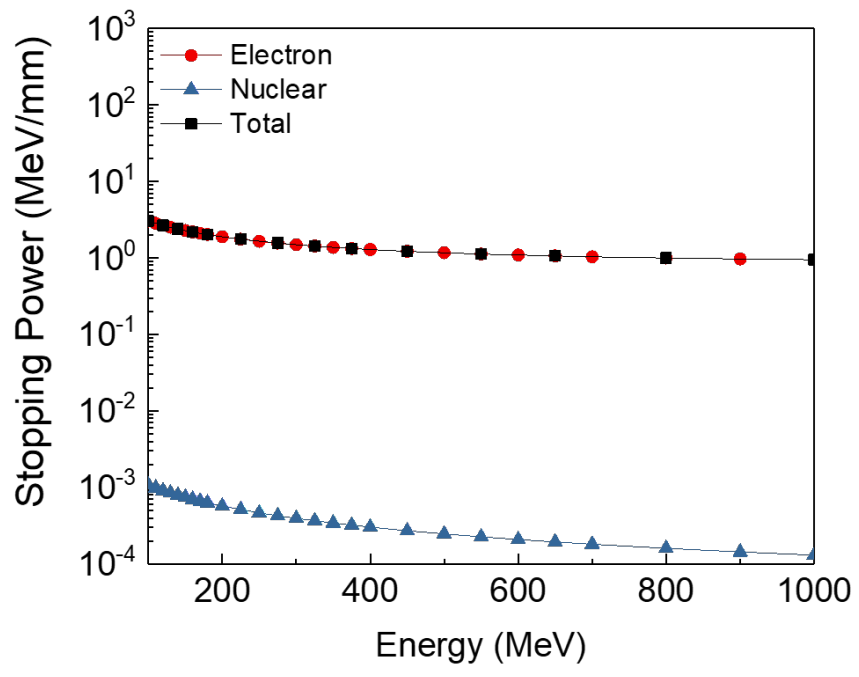


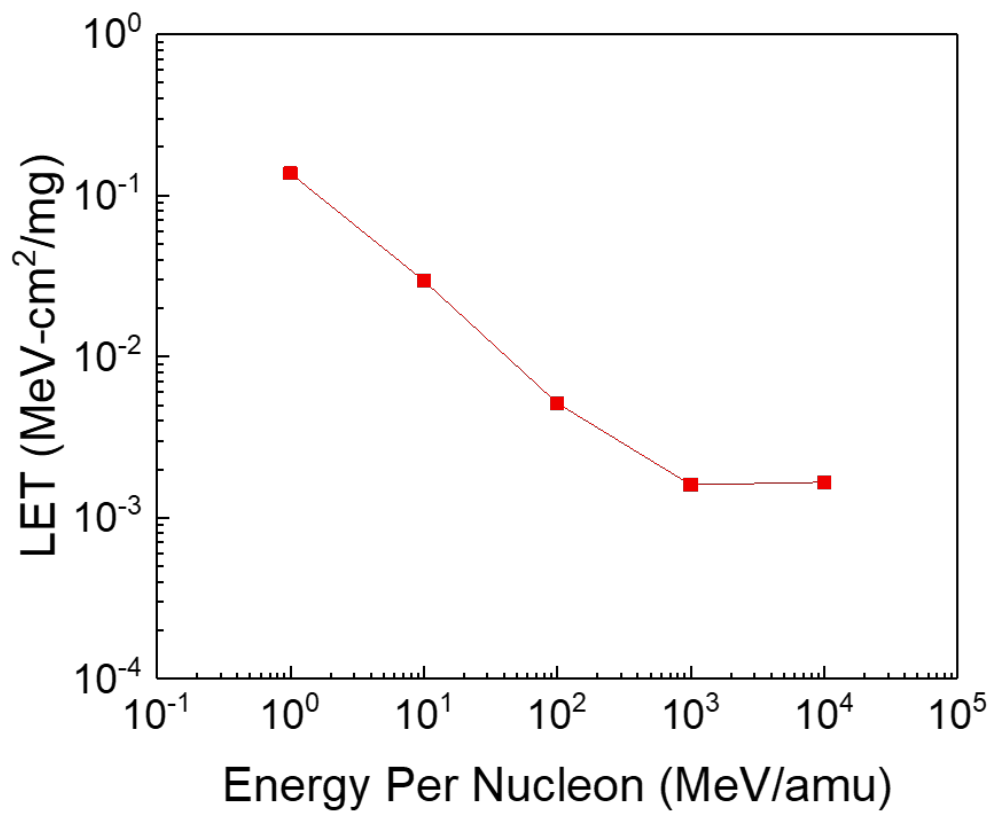
# Displacement Damage











### Irradiation Details:

**Species:**  $^1\text{H}$

25 keV  $1.6 \times 10^{14} \text{ cm}^{-2}$  + 50 keV,  $1.7 \times 10^{14} \text{ cm}^{-2}$  +

70 keV,  $3.6 \times 10^{14} \text{ cm}^{-2}$

